

# Self-Supervised Representation Learning for RGB-D Salient Object Detection

Xiaoqi Zhao<sup>1</sup> Youwei Pang<sup>1</sup> Lihe Zhang<sup>1\*</sup> Huchuan Lu<sup>1,2</sup> Xiang Ruan<sup>3</sup>  
<sup>1</sup>Dalian University of Technology, China  
<sup>2</sup>Peng Cheng Laboratory, China  
<sup>3</sup>Tiwaki Co.,Ltd., Japan

## Abstract

Existing CNNs-Based RGB-D Salient Object Detection (SOD) networks are all required to be pre-trained on the ImageNet to learn the hierarchy features which can help to provide a good initialization. However, the collection and annotation of large-scale datasets are time-consuming and expensive. In this paper, we utilize Self-Supervised Representation Learning (SSL) to design two pretext tasks: the cross-modal auto-encoder and the depth-contour estimation. Our pretext tasks require only a few and unlabeled RGB-D datasets to perform pre-training, which makes the network capture rich semantic contexts and reduce the gap between two modalities, thereby providing an effective initialization for the downstream task. In addition, for the inherent problem of cross-modal fusion in RGB-D SOD, we propose a consistency-difference aggregation (CDA) module that splits a single feature fusion into multi-path fusion to achieve an adequate perception of consistent and differential information. The CDA module is general and suitable for both cross-modal and cross-level feature fusion. Extensive experiments on six benchmark RGB-D SOD datasets, our model pre-trained on the RGB-D dataset (6,392 without any annotations) can perform favorably against most state-of-the-art RGB-D methods pre-trained on ImageNet (1,280,000 with image-level annotations).

## 1. Introduction

RGB-D salient object detection (SOD) task aims to utilize the depth map, which contains stable geometric structures and extra contrast cues, to provide important supplemental information for handling complex environments such as low-contrast salient objects that share similar appearances to the background. Benefiting from Microsoft Kinect, Intel RealSense, and some modern smartphones (e.g., Huawei Mate30, iPhone X, and Samsung Galaxy S20), depth information can be conveniently obtained.

With the development of deep convolutional neural networks (CNNs), many CNNs-Based RGB-D SOD meth-

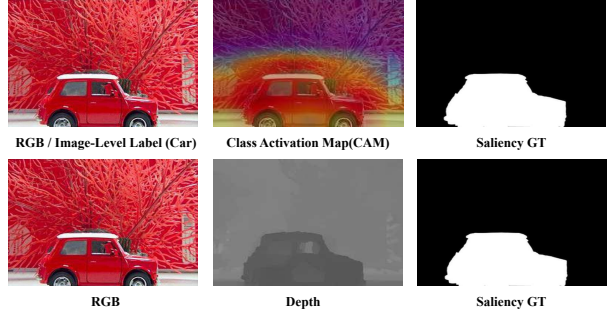


Figure 1: Visual results of classification, depth estimation and salient object detection.

ods [48, 39, 26, 41, 29, 49, 27, 20, 36, 47] can achieve satisfactory performance. They all are required to be pre-trained on the ImageNet [12] to learn rich and high-performance visual representations for downstream tasks. However, the ImageNet contains about 1.3 million labeled images covering 1,000 classes while each image is labeled by human workers with one class label. Such expensive labor costs are immeasurable. Recently, Doersch *et al.* [13], Wang and Gupta [45] and Agrawal *et al.* [2] have explored a novel paradigm for unsupervised learning called self-supervised learning (SSL). The main idea is to exploit different labeling that is freely available besides or within visual data and to use them as intrinsic reward signals to learn general-purpose features. In the learning process, the context has proven to be a powerful source of automatic supervisory signal for learning representations [3, 35, 10, 32]. The SSL needs to design a “pretext” task to learn rich context and then utilizes the pre-trained model for some other “downstream” tasks, such as classification, detection, and semantic segmentation. In addition, for the RGB-D SOD task, how to fully integrate the features of two modalities is still an open problem of great concern, just like the cross-level feature fusion. How to better design a general module suitable for feature pairs with multiple complementary relationships is a currently neglected issue.

Two-stream RGB-D SOD networks [5, 7, 44, 39, 29, 27] usually load ImageNet-pretrained weights. Their encoders for RGB and depth streams have the same pre-training task,

i.e., image classification. Their decoders also have the same task of saliency prediction. This kind of task homogeneousness in both encoder and decoder can greatly reduce the inter-modal gap between the two streams. We know that image classification network often activates the corresponding semantic region in feature maps (e.g., Class Activation Map), while the depth map possibly highlights salient regions, as shown in Fig. 1. Inspired by this, we firstly design a pretext task of depth estimation, which can promote the RGB encoder to capture localization, boundary and shape information of objects by comparing relative spatial positions at the pixel level. Moreover, the depth map plays an information filtering and attention role in RGB-D SOD, which is the same as the class activation map in image classification. Secondly, in order to reinforce the cross-modal information interaction, we design another pretext task of reconstructing RGB channels from the depth map. This task requires that the network learns the way to assign the colors for different positions. Due to the limited prior information, this is a very difficult task, which can stimulate the potential of representation learning and drive the depth encoder to capture the cues of shapes and semantic relationships among different objects and fore/backgrounds. The above two pretext tasks actually form a cross-modal auto-encoder, which only needs pairs of RGB and Depth images without any mutual labels.

In the decoder, we design a pretext task of depth-contour estimation. The reason is twofold: (1) Similar prediction tasks help reduce the gap between the modalities. As shown in Fig. 2, the contour prediction is an analogous process to saliency detection. (2) The depth contour is cleaner than the RGB contour and tends to better depict edge information about salient object/objects, since based on human cognition, salient objects usually have more pronounced depth difference from the background. Moreover, the contour is also an important attribute of salient object. Once the pretext can predict the contour of the salient object well, it simplifies the downstream RGB-D SOD task to predict fore/background properties inside and outside the contour. After these pretext networks have been trained, the RGB-D SOD network can gain good initialization.

About the network architecture, we propose a general module called consistency-difference aggregation (CDA) to achieve both cross-modal and cross-level fusion. Specifically, for two types of features with complementary relationships, we calculate their jointly consistent (JC) features and jointly differential (JD) features. The JC maintains more attention to their consistency and suppresses the interference of non-salient information, while the JD depicts their difference in salient region and encourages the cross-modal or cross-level alignment. By saliency guided consistency-difference aggregation, the gap between modalities or levels is greatly narrowed.

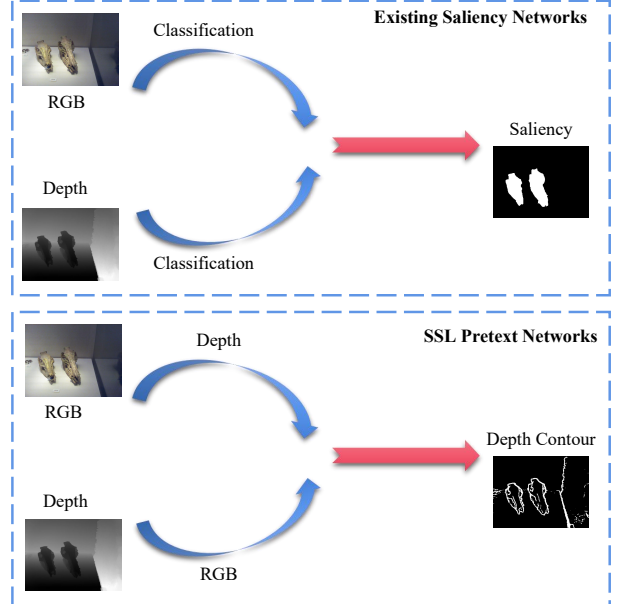


Figure 2: The abstract-analogy of our SSL networks based two-streams RGB-D SOD networks.

Our main contributions can be summarized as follows:

- We present a self-supervised network closely related to the RGB-D SOD task, which consists of a cross-modal auto-encoder and a depth-contour estimation decoder. It is the first method to use self-supervised representation learning for RGB-D SOD.
- We design a simple yet effective consistency-difference aggregation structure that is suitable for both cross-level and cross-modal feature integration.
- We use 6,392 pairs of RGB-Depth images (without manual annotations) to pre-train the model instead of using ImageNet (1,280,000 with image-level labels). Our model still performs much better than most competitors on six RGB-D SOD datasets.

## 2. Related Work

### 2.1. RGB-D Salient Object Detection

Generally speaking, the depth map can be utilized in three ways : early fusion [38, 43, 49], middle fusion [19] and late fusion [18]. According to the number of encoding streams, RGB-D SOD methods can be divided into two-stream [5, 48, 29, 27, 8, 17] and single-stream [49] ones. The two-stream networks mainly focus on sufficiently incorporating cross-modal complementarity. PCANet [5] examines the multi-level fusion between the two streams. Zhao *et al.* [48] feeds RGB images into the RGB-encoder and inserts a shallow convolutional depth-encoder between

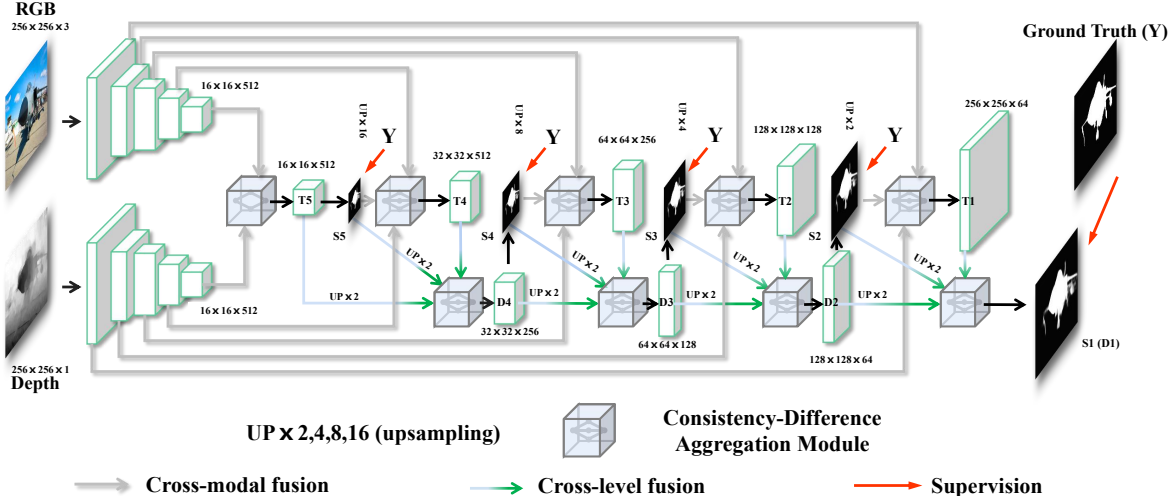


Figure 3: Network pipeline of the downstream task. It consists of two VGG-16 encoders, five cross-modal layers and four decoder blocks. Both the cross-modal and cross-level fusions are achieved by the consistency-difference aggregation (CDA) module. We generate ground truth of multiple resolutions and use cross-entropy loss as supervision.

adjacent encoder blocks to extract the guidance information from the depth map. Liu *et al.* [29] utilize the self-attention and the other modality’s attention in the Non-local structure to fuse multi-modal information. Chen and Fu [8] propose an alternate refinement strategy and combine a guided residual block to generate both refined feature and refined prediction. These two-stream designs significantly increase the number of parameters in the network. Recently, Zhao *et al.* [49] combine depth map and RGB image from starting to build a real single-stream network to take advantage of the potential contrast information provided by the depth map, which provides a new perspective on the RGB-D SOD field. Besides, different level features have different characteristics. High-level ones have more semantic information which helps localize the objects, while low-level ones have more detailed information which can capture the subtle structures of objects. However, both two-stream and single-stream networks belittle the cross-level fusion, which may lead to a significant reduction in the effectiveness of the cross-modal fusion. In this work, we propose a consistency-difference aggregation module, which can be applied in universal combination of multiple complementary relationships (RGB/Depth, High/Low level).

## 2.2. Self-Supervised Representation Learning

Self-supervised learning (SSL) is an important branch of unsupervised learning technique. It refers to the learning paradigm in which ConvNets are explicitly trained with automatically generated labels. During the training phase, a predefined pretext task is designed for ConvNets, and the pseudo labels in the pretext task are automatically generated based on some attributes of data. Then the ConvNet is trained to learn object functions of the pretext task. After the SSL training is finished, the learned weights are trans-

ferred to downstream tasks as their pre-trained models. This strategy can overcome overfitting of small sample problem and obtain the generalization capability of ConvNets.

Many pretext tasks have been designed and applied for self-supervised learning, such as image inpainting [37], clustering [4], image colorization [25], temporal order verification [33] and visual audio correspondence verification [24]. Effective pretext tasks can promote ConvNets to learn useful semantic features for the downstream task. In this work, we rely on the characteristics of RGB-D SOD task to design two related pretext tasks: cross-modal auto-encoder and depth-contour estimation. The former encourages the two-stream encoder to learn each modal information and reduce the inter-modal gap. The latter can further facilitate the cross-modal fusion, which also provides a good feature prior to ease the capture of object-contour and object-localization.

## 3. The Proposed Method

In this section, we first describe the overall architecture of the proposed RGB-D SOD network. And then, we present the details of the consistency-difference aggregation (CDA) module for cross-modal and cross-level feature fusion. Next, we introduce the designed pretext tasks: cross-modal auto-encoder and depth-contour estimation. Finally, we list all the supervisions and loss functions used in the network for both the pretext tasks and the downstream task.

### 3.1. The Overall Architecture

Our network architecture, shown in Fig. 3, follows a two-stream model that consists of five encoder blocks, five transition layers ( $T^i$   $i \in \{1, 2, 3, 4, 5\}$ ), four decoder blocks ( $D^i$   $i \in \{1, 2, 3, 4\}$ ) and nine consistency-difference aggre-

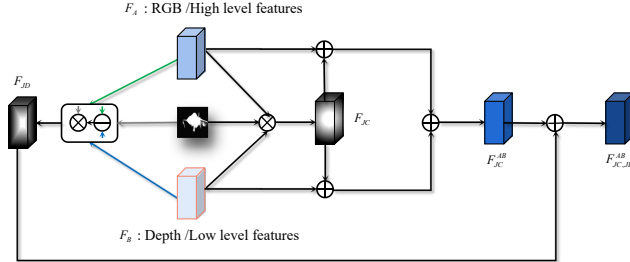


Figure 4: Illustration of the consistency-difference aggregation module.

gation modules. The encoder-decoder architecture is based on the FPN [28]. The encoder is based on a common backbone network, e.g., VGG-16 [42], to perform feature extraction on RGB and Depth, respectively. We cast away all the fully-connected layers and the last pooling layer of the VGG-16 to modify it into a fully convolutional network. We convey the output features from the encoding blocks of two modalities to the consistency-difference aggregation module to achieve cross-modal fusion at each level. And the CDA is also embedded in the decoder. Once these cross-modal fused features are obtained, they will participate in the decoder and gradually integrate the details from high-level to low-level, thereby continuously restoring the full-resolution saliency map.

### 3.2. Consistency-Difference Aggregation Module

The consistency-difference aggregation module can strengthen the consistency of features and highlight their differences, thereby increasing inter-class difference and reducing intra-class difference. Fig. 4 shows the internal structure of the proposed CDA module. We use  $F_A$  and  $F_B$  to represent different modality or level feature maps. They all have been activated by the ReLU operation. First, we use element-wise multiplication between  $F_A$  and  $F_B$  at the same time constrained by saliency map  $S$  of the side-out prediction to obtain high-confidence region features, which are usually consistent with salient objects. This process can be formulated as follows:

$$F_{JC} = \text{Conv}(F_A \otimes F_B \otimes S), \quad (1)$$

where  $\otimes$  is the element-wise multiplication and  $\text{Conv}(\cdot)$  denotes the convolution layer. Next, the jointly consistent features are applied to enhance saliency cues in  $F_A$  and  $F_B$ , thereby yielding initial fused features,

$$F_{JC}^{AB} = \text{Conv}(\text{Conv}(F_{JC} \oplus F_A) \oplus \text{Conv}(F_{JC} \oplus F_B)), \quad (2)$$

where  $\oplus$  is the element-wise addition.  $F_{JC}^{AB}$  achieves consistency boosting of features, especially in salient regions. We calculate the jointly differential features of  $F_A$  and  $F_B$ :

$$F_{JD} = \text{Conv}(|F_A \ominus F_B| \otimes S), \quad (3)$$

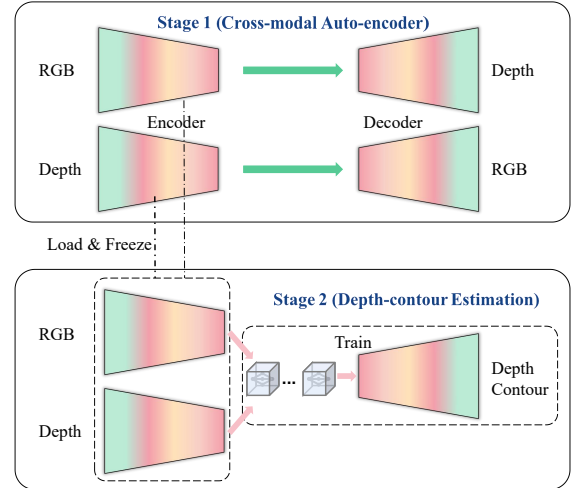


Figure 5: Network pipeline of the pretext tasks. Stage 1: Cross-modal auto-encoder. Stage 2: Depth-contour estimation. The network in Stage 2 is equipped with the CDAs.

where  $\ominus$  is the element-wise subtraction and  $|\cdot|$  calculates the absolute value.  $F_{JD}$  depicts the feature difference in salient regions. The final fusion are generated by combining  $F_{JC}^{AB}$  and  $F_{JD}$ :

$$F_{JC,JD}^{AB} = \text{Conv}(F_{JC}^{AB} \oplus F_{JD}). \quad (4)$$

Compared with  $F_{JC}^{AB}$ ,  $F_{JC,JD}^{AB}$  contains richer complementary information about salient objects. Through a series of addition and subtraction, the features are well aligned under the constraint of the side-out prediction, thereby progressively promoting the correspondence between feature distribution and fore/background categories in the common space, as shown in Fig. 7.

### 3.3. Pretext Tasks: Cross-modal Auto-encoder and Depth-contour Estimation

Instead of previous approaches which obtain effective initial representations through ImageNet pre-training, we design a pure self-supervised network to mine RGB-D information without manual annotations. Fig. 5 shows the structure of the proposed SSL network, which consists of two components, namely, the cross-modal auto-encoder and the depth-contour estimation decoder.

In the first stage, we use pairs of RGB-Depth data to predict each other, i.e., using the RGB image to predict the depth map and using the depth map to reconstruct the RGB image. The backbone of these two networks is based on VGG-16 with random initialization. We directly adopt the FPN as the basic structure. Through the cross-modal auto-encoder, the encoder of the RGB or depth stream can respectively turn to capture the information of another modal. As a result, the features of the two encoders tend to converge into a common space, which greatly reduces the gap

between modalities to facilitate subsequent cross-modal fusion. Moreover, in the process of predicting each other, the contextual representation capabilities can be effectively learned in their own streams. As suggested in [21], increasing the complexity of the pretext task is generally beneficial to the performance of the SSL. In this work, our cross-modal encoders do not interact with each other in any way. The completely independent cross-modal generation obviously elevates the difficulty, making the network try its best to learn useful semantic cues about the two modalities.

In the second stage, we load the parameters of the encoders trained in the first stage to calculate multi-scale features in each encoding stream. And then, we exploit the designed CDA module described in Sec. 3.2 to achieve the cross-modal and cross-level fusion for predicting the depth-contour. This pretext task allows further cross-modal integration, and the learned features provide contour prior (i.e., a kind of fore/background semantic guidance) for the downstream task to predict saliency map.

### 3.4. Supervision

In the proposed RGB-D SOD network, the total training loss can be written as:

$$L_{sod} = \sum_{n=1}^N l_{bce}^{(n)}, \quad (5)$$

where  $l_{bce}$  is the BCE loss [11], which is widely used in binary segmentation.  $N$  denotes the number of the side-out. As described in Sec. 3.2, our RGB-D SOD model is deeply supervised with five outputs, i.e.  $N = 5$ . The BCE loss can be computed as:

$$l_{bce} = -(Y \log P + (1 - Y) \log(1 - P)), \quad (6)$$

where  $P$  and  $Y$  denote the predicted map and ground truth, respectively.

The cross-modal auto-encoder task consists of depth estimation and RGB reconstruction. Both of them are trained by using the SSIM-loss and the L1-loss. SSIM is originally proposed for image quality assessment [46]. It can capture the structural information in an image. Since both RGB and depth information presents patch consistency in a scene, the use of SSIM is well suited as a loss function for the patch-level regularization. Let  $x = \{x_i : i = 1, \dots, N^2\}$  and  $y = \{y_i : i = 1, \dots, N^2\}$  be the pixel values of two patches (size:  $N \times N$ ) cropped from the predicted predicted map  $X$  and the ground truth  $Y$ , respectively, the SSIM-loss of  $x$  and  $y$  is defined as:

$$l_{ssim} = 1 - \frac{(2\mu_x\mu_y + C_1)(2\sigma_{xy} + C_2)}{(\mu_x^2 + \mu_y^2 + C_1)(\sigma_x^2 + \sigma_y^2 + C_2)}, \quad (7)$$

where  $\mu_x$ ,  $\mu_y$  and  $\sigma_x$ ,  $\sigma_y$  denote the mean and standard deviations of  $x$  and  $y$ , respectively, and  $\sigma_{xy}$  is their covariance.

$C_1 = 0.012$  and  $C_2 = 0.032$  are used to avoid dividing by zero. The L1-loss calculates the absolute distance between the predicted map and ground truth, which is supervised at the pixel-level:

$$l_1 = |P - Y|. \quad (8)$$

Finally, the total loss of both depth estimation and RGB reconstruction is as follow:

$$L_{d/rgb} = \sum_{n=1}^N (l_{ssim}^{(n)} + l_1^{(n)}). \quad (9)$$

The combination of SSIM-loss and L1-loss allows the network to have both patch-level and pixel-level supervision, thereby promoting more locally consistent prediction.

For the depth-contour estimation task, its ground truth ( $G_{dc}$ ) is calculated based on the depth map ( $G_d$ ) provided by the RGB-D datasets. Specifically, we employ the morphological dilation and erosion as follows:

$$G_{dc} = D_m(G_d) - E_m(G_d), \quad (10)$$

where  $D(\cdot)$  and  $E(\cdot)$  are the dilation and erosion operations, respectively.  $m$  denotes a full one filter of size  $m \times m$  for erosion and expansion. It is set to 5 in this paper. We only use the L1-loss for each side-out during the training phase.

## 4. Experiments

### 4.1. Datasets

We evaluate the proposed model on six public RGB-D SOD datasets which are *RGBD135* [9], *DUT-RGBD* [39], *STERE* [34], *NLPR* [38], *NJUD* [23] and *SIP* [16]. For the downstream task, we adopt the same training set as most methods [39, 26, 41, 29, 49, 27], that is, 800 samples from the DUT-RGBD, 1,485 samples from the NJUD and 700 samples from the NLPR are used for training. The remaining images and other three datasets are used for testing. For the pretext tasks, we combine training subsets of NJUD and NLPR with the recent DUTLF-V2 [40] (4,207 samples) to finish pre-training, that is, 6,392 training images in total.

### 4.2. Evaluation Metrics

We adopt several widely used metrics for quantitative evaluation: F-measure ( $F_\beta^{max}$ ) [1], the weighted F-measure ( $F_\beta^w$ ) [31], mean absolute error (MAE,  $\mathcal{M}$ ), the recently released S-measure ( $S_m$ ) [14] and E-measure ( $E_m$ ) [15] scores. The lower value is better for the MAE and the higher is better for others.

### 4.3. Implementation Details

We first use random initialization to train the SSL cross-modal auto-encoder. And then the parameters of the encoder of each stream are loaded for the following depth-contour estimation. In this process, the parameters of the

two-stream encoder are frozen, we only train the decoder with the CDA modules. Once the pretext tasks are finished, we load their parameters to initialize the network for the downstream task (RGB-D SOD).

Our models are implemented based on the Pytorch and trained on a RTX 2080Ti GPU for 50 epochs with mini-batch size 4. We adopt some data augmentation techniques to avoid overfitting: random horizontally flipping, random rotate, random brightness, saturation and contrast. For the optimizer, we use the stochastic gradient descent (SGD) with a momentum of 0.9 and a weight decay of 0.0005. For the pretext tasks, the learning rate is set to 0.001 and later use the “poly” policy [30] with the power of 0.9 as a means of adjustment. For the downstream task, maximum learning rate is set to 0.005 for backbone and 0.05 for other parts. Warm-up and linear decay strategies are used to adjust the learning rate.

#### 4.4. Comparisons with State-of-the-art

The proposed algorithm is compared with eleven state-of-the-art methods. For fair comparisons, all saliency maps of these competitors are directly provided by their respective authors or computed by their released codes.

**Quantitative Evaluation.** Tab. 1 shows performance comparisons in terms of the F-measure, weighted F-measure, S-measure, E-measure and MAE scores. According to the proportion of each testing set to all testing sets, the results on all datasets are weighted and summed to obtain an overall performance evaluation, which is listed in the row “Ave-Metric”. It can be seen that our fully supervised (i.e., ImageNet pre-trained) model ranks first among thirteen models in the overall ranking. It is the only method that exceeds 0.85 and 0.90 in terms of the weighted F-measure and S-measure, respectively. Notably, our self-supervised model outperforms all other fully supervised methods and ranks second among them, which shows the great potential of self-supervised learning and the effectiveness of the pretext tasks we design.

**Qualitative Evaluation.** Fig. 6 illustrates the visual comparison with other RGB-D SOD approaches. The proposed method yields the results closer to the ground truth in various challenging scenarios. For the images with a single object, our method can completely segment the whole object, while other competitors lose more or less parts of the object (see the 1<sup>st</sup> - 3<sup>th</sup> rows). For images having multiple objects, our method can still accurately localize and capture all the objects (see the 4<sup>th</sup> and 5<sup>th</sup> rows). Moreover, it can be seen that our SSL model even has better visual results compared to other fully supervised methods.

#### 4.5. Ablation Study

In this section, we detail the contribution of each component to the overall network. We first verify the effectiveness

of the CDA module when the RGB-D SOD networks are pre-trained on the ImageNet. Next, we evaluate the SSL pretext networks by loading different pre-trained parameters to the RGB-D SOD network, the performance gain illustrates the benefits of the proposed SSL pretexts. All ablation experiments are based on the VGG-16 backbone.

##### Effectiveness of Consistency-Difference Aggregation.

In Tab. 2, we show the performance contributed by different structures on all RGB-D SOD datasets in terms of the weighted average metrics “Ave-Metric”. The baseline (Model 1) is a two-stream FPN structure with deep supervision. We can see that this baseline has been able to rank eighth in Tab. 1. Based on this strong baseline, the performance gain is more convincing. Model 2 vs. Model 1 and Model 4 vs. Model 1 show the effectiveness of the jointly consistent features (JC) in cross-modal and cross-level integration, respectively. The JC can significantly improve the performance. Similarly, Model 3 vs. Model 2 and Model 5 vs. Model 4 show the advantages of the jointly differential features (JD). Model 6 is equipped with the CDA module in both the cross-modal and cross-level fusion. Model 6 vs. Model 3 and Model 6 vs. Model 5 demonstrate the generalization of the CDA in the two kinds of information fusion, which complement each other without repulsion. To further evaluate the rationality of this module, the CDA is replaced with some operations of addition and convolution and a similar number of parameters are preserved. This new network is noted as Model 7. Compared to it, Model 6 has obvious advantages on performance.

We visualize intermediate features in the CDA module as shown in Fig 7. By explicitly superposing the influence of the cross-modal (or cross-level) joint consistency  $F_{JC}$  and joint difference  $F_{JD}$  under the constraint of saliency map, the fused feature  $F_{JC,JD}^{RGB,D}$  (or  $F_{JC,JD}^{4,3}$ ) can highlight salient regions well. Thus, the network equipped with the CDAs can more completely extract salient objects, whereas the network without the CDA is disturbed by a large number of non-salient areas (see the third row in Fig 7). More comparisons are shown in the supplementary material.

##### Effectiveness of Self-supervised Pre-training.

In Tab. 3, we evaluate the effectiveness of the proposed SSL pretexts on the RGB-D SOD task in terms of the weighted average metrics “Ave-Metric”. Firstly, we train the first pretext (P1), cross-modal auto-encoder. As shown in Fig. 8, the predicted depth maps are close to the GT and the reconstructed RGB images clearly fit the semantics of the original images, such as the sky becomes blue and even the cat is colored with white. Next, we load the pre-trained parameters from P1 to jointly train the second pretext (P2), depth-contour estimation. The visual results are shown in Fig. 8. Model 2 vs. Model 1 shows that the P1 task can significantly improve the representation capability of the two-stream encoder. Model 5 vs. Model 4 and Model 7

Table 1: Quantitative comparison of different RGB-D SOD methods.  $\uparrow$  and  $\downarrow$  indicate that the larger scores and the smaller ones are better, respectively. The best three results are shown in **red**, **green** and **blue**. The subscript in each model name is the publication year.

Metric	Fully-supervised (Pre-trained on the ImageNet)											Self-supervised Ours		
	CTMF <sub>18</sub> [22]	PCANet <sub>18</sub> [5]	MMCI <sub>19</sub> [7]	TANet <sub>19</sub> [39]	CPFP <sub>19</sub> [6]	DMRA <sub>19</sub> [48]	ICNet <sub>20</sub> [26]	A2DELE <sub>20</sub> [41]	S2MA <sub>20</sub> [29]	DANet <sub>20</sub> [49]	CMWNet <sub>20</sub> [27]			
RGBD35 [9]	$F_{\beta}^{max} \uparrow$ 0.865	0.842	0.839	0.853	0.882	0.906	0.925	0.897	<b>0.944</b>	0.916	0.939	<b>0.946</b>	<b>0.945</b>	
	$F_{\beta}^w \uparrow$ 0.687	0.711	0.650	0.740	0.787	0.843	0.867	0.836	<b>0.892</b>	0.848	0.888	<b>0.906</b>	<b>0.902</b>	
	$S_m \uparrow$ 0.863	0.843	0.848	0.858	0.872	0.899	0.920	0.886	<b>0.941</b>	0.905	0.934	<b>0.936</b>	<b>0.940</b>	
	$E_m \uparrow$ 0.911	0.912	0.904	0.919	0.927	0.944	0.959	0.920	<b>0.974</b>	0.961	0.967	<b>0.978</b>	<b>0.979</b>	
	$\mathcal{M} \downarrow$ 0.055	0.050	0.065	0.046	0.038	0.030	0.027	0.029	<b>0.021</b>	0.028	0.022	<b>0.018</b>	<b>0.019</b>	
DUT-RGBD [39]	$F_{\beta}^{max} \uparrow$ 0.842	0.809	0.804	0.823	0.787	0.908	0.875	0.907	0.909	<b>0.911</b>	0.905	<b>0.929</b>	<b>0.922</b>	
	$F_{\beta}^w \uparrow$ 0.682	0.688	0.628	0.705	0.638	0.852	0.784	<b>0.864</b>	0.862	0.847	0.831	<b>0.879</b>	<b>0.866</b>	
	$S_m \uparrow$ 0.831	0.801	0.791	0.808	0.749	0.887	0.852	0.886	<b>0.903</b>	<b>0.889</b>	0.887	<b>0.912</b>	<b>0.903</b>	
	$E_m \uparrow$ 0.883	0.863	0.856	0.871	0.815	<b>0.930</b>	0.901	0.929	0.921	0.929	0.922	<b>0.943</b>	<b>0.937</b>	
	$\mathcal{M} \downarrow$ 0.097	0.100	0.112	0.093	0.100	0.048	0.072	<b>0.043</b>	0.044	0.047	0.056	<b>0.038</b>	<b>0.041</b>	
STERE [34]	$F_{\beta}^{max} \uparrow$ 0.848	0.875	0.877	0.878	0.889	0.802	<b>0.908</b>	0.892	0.895	0.897	<b>0.911</b>	<b>0.915</b>	0.904	
	$F_{\beta}^w \uparrow$ 0.698	0.778	0.760	0.787	0.817	0.647	0.844	<b>0.846</b>	0.825	0.830	<b>0.847</b>	<b>0.860</b>	0.833	
	$S_m \uparrow$ 0.848	0.875	0.873	0.871	0.879	0.752	<b>0.903</b>	0.878	0.890	0.892	<b>0.905</b>	<b>0.906</b>	0.890	
	$E_m \uparrow$ 0.870	0.907	0.905	0.916	0.907	0.816	0.926	<b>0.928</b>	0.926	0.927	<b>0.930</b>	<b>0.930</b>	<b>0.932</b>	
	$\mathcal{M} \downarrow$ 0.086	0.064	0.068	0.060	0.051	0.087	<b>0.045</b>	<b>0.045</b>	0.051	0.048	<b>0.043</b>	<b>0.040</b>	0.047	
NLPR [38]	$F_{\beta}^{max} \uparrow$ 0.841	0.864	0.841	0.876	0.884	0.888	<b>0.919</b>	0.898	0.910	0.908	0.913	<b>0.925</b>	<b>0.920</b>	
	$F_{\beta}^w \uparrow$ 0.679	0.762	0.676	0.780	0.807	0.840	<b>0.864</b>	0.857	0.852	0.850	0.856	<b>0.885</b>	<b>0.862</b>	
	$S_m \uparrow$ 0.860	0.874	0.856	0.886	0.884	0.898	<b>0.922</b>	0.898	0.915	0.908	<b>0.917</b>	<b>0.929</b>	0.916	
	$E_m \uparrow$ 0.869	0.916	0.872	0.916	0.920	0.942	<b>0.945</b>	<b>0.945</b>	0.942	<b>0.945</b>	0.941	<b>0.958</b>	<b>0.950</b>	
	$\mathcal{M} \downarrow$ 0.056	0.044	0.059	0.041	0.038	0.031	<b>0.028</b>	<b>0.029</b>	0.030	0.031	<b>0.029</b>	<b>0.023</b>	<b>0.029</b>	
NUD [23]	$F_{\beta}^{max} \uparrow$ 0.857	0.888	0.868	0.888	0.890	0.896	0.902	0.890	0.899	0.905	<b>0.913</b>	<b>0.916</b>	<b>0.919</b>	
	$F_{\beta}^w \uparrow$ 0.720	0.803	0.739	0.805	0.828	0.847	0.843	0.843	0.842	0.853	<b>0.857</b>	<b>0.872</b>	<b>0.866</b>	
	$S_m \uparrow$ 0.849	0.877	0.859	0.878	0.878	0.885	0.894	0.871	0.894	0.897	<b>0.903</b>	<b>0.910</b>	<b>0.907</b>	
	$E_m \uparrow$ 0.866	0.909	0.882	0.909	0.900	0.920	0.913	0.916	0.917	<b>0.926</b>	<b>0.923</b>	0.916	<b>0.935</b>	
	$\mathcal{M} \downarrow$ 0.085	0.059	0.079	0.061	0.053	0.051	0.052	0.051	0.053	<b>0.046</b>	<b>0.046</b>	<b>0.041</b>	<b>0.042</b>	
SIP [16]	$F_{\beta}^{max} \uparrow$ 0.720	0.861	0.840	0.851	0.870	0.847	0.873	0.855	<b>0.891</b>	<b>0.901</b>	0.890	<b>0.903</b>	0.887	
	$F_{\beta}^w \uparrow$ 0.535	0.768	0.712	0.748	0.788	0.734	0.791	0.780	<b>0.819</b>	<b>0.829</b>	0.811	<b>0.841</b>	0.803	
	$S_m \uparrow$ 0.716	0.842	0.833	0.835	0.850	0.800	0.854	0.828	<b>0.872</b>	<b>0.878</b>	0.867	<b>0.884</b>	0.858	
	$E_m \uparrow$ 0.824	0.900	0.886	0.894	0.899	0.858	0.900	0.890	<b>0.913</b>	<b>0.917</b>	0.909	<b>0.919</b>	0.899	
	$\mathcal{M} \downarrow$ 0.139	0.071	0.086	0.075	0.064	0.088	0.070	0.070	<b>0.057</b>	<b>0.054</b>	0.062	<b>0.050</b>	0.064	
Ave-Metric	$F_{\beta}^{max} \uparrow$ 0.812	0.862	0.851	0.864	0.870	0.854	0.895	0.884	0.900	0.903	<b>0.906</b>	<b>0.916</b>	<b>0.907</b>	
	$F_{\beta}^w \uparrow$ 0.651	0.764	0.715	0.766	0.786	0.753	0.824	0.830	0.835	<b>0.838</b>	<b>0.839</b>	<b>0.863</b>	<b>0.839</b>	
	$S_m \uparrow$ 0.810	0.855	0.847	0.855	0.855	0.822	0.884	0.866	<b>0.892</b>	0.891	<b>0.894</b>	<b>0.904</b>	0.889	
	$E_m \uparrow$ 0.859	0.901	0.887	0.903	0.895	0.875	0.917	0.917	<b>0.924</b>	<b>0.927</b>	<b>0.924</b>	<b>0.931</b>	<b>0.927</b>	
	$\mathcal{M} \downarrow$ 0.098	0.067	0.079	0.066	0.059	0.069	0.054	0.050	0.049	<b>0.047</b>	<b>0.048</b>	<b>0.040</b>	<b>0.047</b>	
Ave - Rank		13	10	12	8	8	11	7	6	5	4	3	1	2

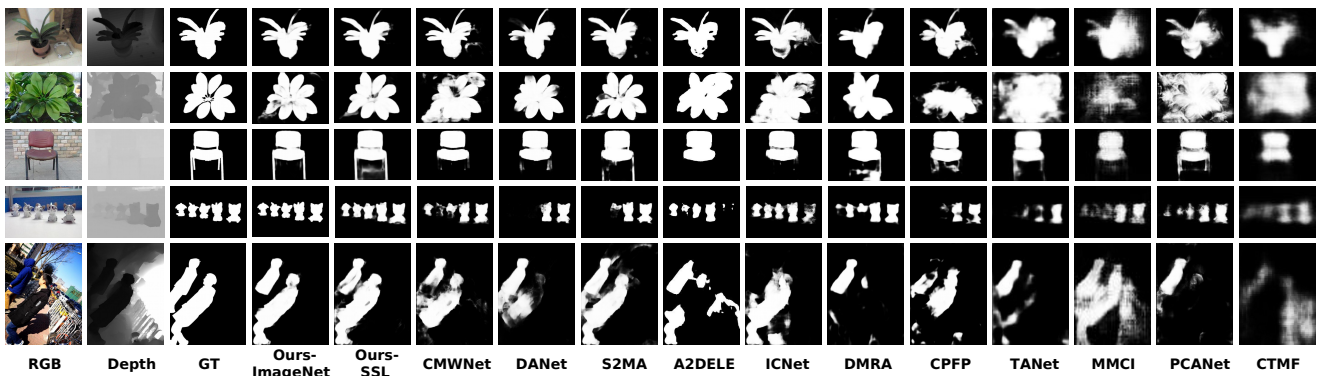


Figure 6: Visual comparison of different RGB-D SOD methods.

Table 2: Ablation experiments of the CDA module.  $B_i$ : Baseline with the ImageNet-pretrained backbone. + CM<sub>jc</sub> and + CL<sub>jc</sub>: Using the joint consistency features in the cross-modal and cross-level fusion, respectively. + CM<sub>jd</sub> and + CL<sub>jd</sub>: Using the joint difference features in the cross-modal and cross-level fusion, respectively.

No.	$B_i$	+ CM <sub>jc</sub>	+ CM <sub>jd</sub>	+ CL <sub>jc</sub>	+ CL <sub>jd</sub>	$F_{\beta}^{max}$	$F_{\beta}^w$	$S_m$	$E_m$	$\mathcal{M}$	Params (MB)
Model 1	✓					0.885	0.799	0.874	0.911	0.057	36.50
Model 2	✓	✓				0.892	0.813	0.882	0.917	0.053	47.50
Model 3	✓	✓	✓			0.897	0.828	0.889	0.920	0.050	58.49
Model 4	✓			✓		0.899	0.827	0.888	0.921	0.050	45.91
Model 5	✓			✓	✓	0.900	0.833	0.890	0.924	0.048	52.18
Model 6	✓	✓	✓	✓	✓	<b>0.916</b>	<b>0.863</b>	<b>0.904</b>	<b>0.931</b>	<b>0.040</b>	74.17
Model 7	✓					0.884	0.815	0.877	0.922	0.053	78.15

Table 3: Ablation experiments of the SSL pretext tasks. All the results are based on the RGB-D SOD network.  $B_r$ : Baseline with the randomly initialized backbone. +P1: Initializing the encoder pretrained in pretext 1 (cross-modal auto-encoder). +P2: Initializing the cross-modal layer and the decoder pretrained in pretext 2 (depth-contour estimation). + CM and + CL: Using the CDA in the cross-modal and cross-level fusion, respectively.

No.	$B_r$	+ P1	+ P2	+ CM	+ CL	$F_{\beta}^{max}$	$F_{\beta}^w$	$S_m$	$E_m$	$\mathcal{M}$
Model 1	✓					0.839	0.712	0.831	0.871	0.087
Model 2	✓	✓				0.865	0.764	0.854	0.898	0.068
Model 3	✓	✓	✓			0.865	0.769	0.857	0.898	0.066
Model 4	✓	✓		✓		0.875	0.789	0.862	0.906	0.062
Model 5	✓	✓	✓	✓		0.882	0.803	0.869	0.913	0.057
Model 6	✓	✓			✓	0.885	0.808	0.873	0.912	0.057
Model 7	✓	✓	✓		✓	0.894	0.816	0.881	0.914	0.054
Model 8	✓			✓	✓	0.863	0.762	0.851	0.889	0.072
Model 9	✓	✓	✓	✓	✓	<b>0.907</b>	<b>0.839</b>	<b>0.889</b>	<b>0.927</b>	<b>0.047</b>

Table 4: Average performance of the SSL-based network with varying number of pre-training examples.

Model	$F_g^{max}$	$F_g^w$	$S_m$	$E_m$	$\mathcal{M}$	Ave - Rank
Random Initialization	0.863	0.762	0.851	0.889	0.072	10
NJUD + NLPR ~2,000	0.895	0.822	0.879	0.917	0.053	5
NJUD + NLPR + DUTLF-V2 (part) ~4,000	0.902	0.831	0.886	0.923	0.050	4
NJUD + NLPR + DUTLF-V2 ~6,000	0.907	0.839	0.889	0.927	0.047	2

vs. Model 6 demonstrate the effectiveness of the P2 task, which averagely improves the performance by 1.38% and 6.66% in terms of the weighted F-measure and MAE, respectively. In addition, Model 4 vs. Model 2 and Model 5 vs. Model 3 can further verify the effect of the CDA in the cross-modal fusion. While Model 6 vs. Model 2 and Model 7 vs. Model 3 show its benefits in the cross-level fusion. Finally, Model 9 vs. Model 8 indicates the overall contribution of two self-supervised learning pretexts. It can be seen that the performance is significantly improved with the gain of 10.10% and 34.72% in terms of the weighted F-measure and MAE, respectively. More comparisons can be found in the supplementary material.

**Evaluation of The Scale of Pre-training Data.** In Tab. 4, we list the performance of using different numbers of SSL training images. We successively add 2,185 training samples of NJUD and NLPR, 2,000 samples of DUTLF-V2 and the rest 2,207 ones of DUTLF-V2 to the training set. We train three SSL networks on  $\sim 2,000 - \sim 6,000$  unlabeled samples, and then load their parameters to initialize the downstream network, respectively. We can see that

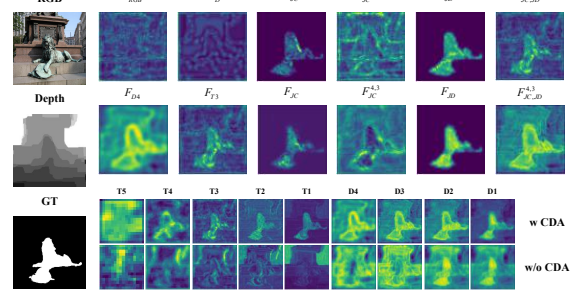


Figure 7: Illustration of the benefits of using the CDA. The first two rows correspond to different intermediate features in Fig. 4 in the cross-modal fusion and cross-level fusion, respectively. The third row shows visual comparison between the features of each level w and w/o CDA.

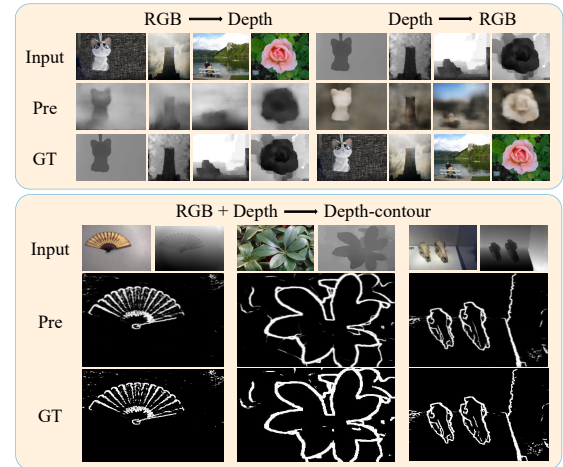


Figure 8: Visual results of the pretext tasks: cross-modal auto-encoder and depth-contour estimation.

when only  $\sim 2,000$  samples are used, the SSL-based network already significantly outperforms the randomly initialized network. With the increasing of training data, the performance is steadily improved, which shows that our SSL model has great potential. More comparisons can be found in the supplementary material.

## 5. Conclusion

In this work, we propose a novel self-supervised learning (SSL) scheme to accomplish effective pre-training for RGB-D SOD without requiring human annotation. The SSL pretext tasks contain cross-modal auto-encoder and depth-contour estimation, by which the network can capture rich context and reduce the gap between modalities. Besides, we design a consistency-difference aggregation module to combine cross-modal and cross-level information. Extensive experiments show our model performs well on RGB-D SOD datasets. As the first method of SSL in RGB-D SOD, it can be taken as a new baseline for future research.

## References

[1] Radhakrishna Achanta, Sheila Hemami, Francisco Estrada, and Sabine Süsstrunk. Frequency-tuned salient region detection. In *CVPR*, pages 1597–1604, 2009.

[2] Pulkit Agrawal, Joao Carreira, and Jitendra Malik. Learning to see by moving. In *ICCV*, pages 37–45, 2015.

[3] Rie Kubota Ando and Tong Zhang. A framework for learning predictive structures from multiple tasks and unlabeled data. *Journal of Machine Learning Research*, 6(Nov):1817–1853, 2005.

[4] Mathilde Caron, Piotr Bojanowski, Armand Joulin, and Matthijs Douze. Deep clustering for unsupervised learning of visual features. In *ECCV*, pages 132–149, 2018.

[5] Hao Chen and Youfu Li. Progressively complementarity-aware fusion network for rgb-d salient object detection. In *CVPR*, pages 3051–3060, 2018.

[6] Hao Chen and Youfu Li. Three-stream attention-aware network for rgb-d salient object detection. *IEEE TIP*, 28(6):2825–2835, 2019.

[7] Hao Chen, Youfu Li, and Dan Su. Multi-modal fusion network with multi-scale multi-path and cross-modal interactions for rgb-d salient object detection. *Pattern Recognition*, 86:376–385, 2019.

[8] Shuhan Chen and Yun Fu. Progressively guided alternate refinement network for rgb-d salient object detection. In *ECCV*, pages 520–538, 2020.

[9] Yupeng Cheng, Huazhu Fu, Xingxing Wei, Jiangjian Xiao, and Xiaochun Cao. Depth enhanced saliency detection method. In *International Conference on Internet Multimedia Computing and Service*, page 23, 2014.

[10] Ronan Collobert and Jason Weston. A unified architecture for natural language processing: Deep neural networks with multitask learning. In *ICML*, pages 160–167, 2008.

[11] Pieter-Tjerk De Boer, Dirk P Kroese, Shie Mannor, and Reuven Y Rubinstein. A tutorial on the cross-entropy method. *Annals of operations research*, 134(1):19–67, 2005.

[12] Jia Deng, Wei Dong, Richard Socher, Li-Jia Li, Kai Li, and Li Fei-Fei. Imagenet: A large-scale hierarchical image database. In *CVPR*, pages 248–255, 2009.

[13] Carl Doersch, Abhinav Gupta, and Alexei A Efros. Unsupervised visual representation learning by context prediction. In *ICCV*, pages 1422–1430, 2015.

[14] Deng-Ping Fan, Ming-Ming Cheng, Yun Liu, Tao Li, and Ali Borji. Structure-measure: A new way to evaluate foreground maps. In *ICCV*, pages 4548–4557, 2017.

[15] Deng-Ping Fan, Cheng Gong, Yang Cao, Bo Ren, Ming-Ming Cheng, and Ali Borji. Enhanced-alignment measure for binary foreground map evaluation. *arXiv preprint arXiv:1805.10421*, 2018.

[16] Deng-Ping Fan, Zheng Lin, Jia-Xing Zhao, Yun Liu, Zhao Zhang, Qibin Hou, Menglong Zhu, and Ming-Ming Cheng. Rethinking rgb-d salient object detection: Models, datasets, and large-scale benchmarks. *arXiv preprint arXiv:1907.06781*, 2019.

[17] Deng-Ping Fan, Yingjie Zhai, Ali Borji, Jufeng Yang, and Ling Shao. Bbs-net: Rgb-d salient object detection with a bifurcated backbone strategy network. In *ECCV*, pages 275–292, 2020.

[18] Xingxing Fan, Zhi Liu, and Guangling Sun. Salient region detection for stereoscopic images. In *International Conference on Digital Signal Processing*, pages 454–458, 2014.

[19] David Feng, Nick Barnes, Shaodi You, and Chris McCarthy. Local background enclosure for rgb-d salient object detection. In *CVPR*, pages 2343–2350, 2016.

[20] Keren Fu, Deng-Ping Fan, Ge-Peng Ji, and Qijun Zhao. Jl-dcf: Joint learning and densely-cooperative fusion framework for rgb-d salient object detection. In *CVPR*, pages 3052–3062, 2020.

[21] Priya Goyal, Dhruv Mahajan, Abhinav Gupta, and Ishan Misra. Scaling and benchmarking self-supervised visual representation learning. In *CVPR*, pages 6391–6400, 2019.

[22] Junwei Han, Hao Chen, Nian Liu, Chenggang Yan, and Xuelong Li. Cnns-based rgb-d saliency detection via cross-view transfer and multiview fusion. *IEEE Transactions on Cybernetics*, 48(11):3171–3183, 2017.

[23] Ran Ju, Ling Ge, Wenjing Geng, Tongwei Ren, and Gangshan Wu. Depth saliency based on anisotropic center-surround difference. In *ICIP*, pages 1115–1119, 2014.

[24] Bruno Korbar, Du Tran, and Lorenzo Torresani. Cooperative learning of audio and video models from self-supervised synchronization. In *NeurIPS*, pages 7763–7774, 2018.

[25] Gustav Larsson, Michael Maire, and Gregory Shakhnarovich. Colorization as a proxy task for visual understanding. In *CVPR*, pages 6874–6883, 2017.

[26] Gongyang Li, Zhi Liu, and Haibin Ling. Icnet: Information conversion network for rgb-d based salient object detection. *IEEE TIP*, 29:4873–4884, 2020.

[27] Gongyang Li, Zhi Liu, Linwei Ye, Yang Wang, and Haibin Ling. Cross-modal weighting network for rgb-d salient object detection. In *ECCV*, pages 665–681, 2020.

[28] Tsung-Yi Lin, Piotr Dollár, Ross Girshick, Kaiming He, Bharath Hariharan, and Serge Belongie. Feature pyramid networks for object detection. In *CVPR*, pages 2117–2125, 2017.

[29] Nian Liu, Ni Zhang, and Junwei Han. Learning selective self-mutual attention for rgb-d saliency detection. In *CVPR*, pages 13756–13765, 2020.

[30] Wei Liu, Andrew Rabinovich, and Alexander C Berg. Parsenet: Looking wider to see better. *arXiv preprint arXiv:1506.04579*, 2015.

[31] Ran Margolin, Lihi Zelnik-Manor, and Ayallet Tal. How to evaluate foreground maps? In *CVPR*, pages 248–255, 2014.

[32] Tomas Mikolov, Ilya Sutskever, Kai Chen, Greg S Corrado, and Jeff Dean. Distributed representations of words and phrases and their compositionality. In *NeurIPS*, pages 3111–3119, 2013.

[33] Ishan Misra, C Lawrence Zitnick, and Martial Hebert. Shuffle and learn: unsupervised learning using temporal order verification. In *ECCV*, pages 527–544, 2016.

[34] Yuzhen Niu, Yujie Geng, Xueqing Li, and Feng Liu. Leveraging stereopsis for saliency analysis. In *CVPR*, pages 454–461, 2012.

[35] Daisuke Okanohara and Jun’ichi Tsuji. A discriminative language model with pseudo-negative samples. In *Proceedings of the 45th Annual Meeting of the Association of Computational Linguistics*, pages 73–80, 2007.

[36] Youwei Pang, Lihe Zhang, Xiaoqi Zhao, and Huchuan Lu. Hierarchical dynamic filtering network for rgb-d salient object detection. In *ECCV*, pages 235–252, 2020.

[37] Deepak Pathak, Philipp Krahenbuhl, Jeff Donahue, Trevor Darrell, and Alexei A Efros. Context encoders: Feature learning by inpainting. In *CVPR*, pages 2536–2544, 2016.

[38] Houwen Peng, Bing Li, Weihua Xiong, Weiming Hu, and Rongrong Ji. Rgbd salient object detection: A benchmark and algorithms. In *ECCV*, pages 92–109, 2014.

[39] Yongri Piao, Wei Ji, Jingjing Li, Miao Zhang, and Huchuan Lu. Depth-induced multi-scale recurrent attention network for saliency detection. In *ICCV*, pages 7254–7263, 2019.

[40] Yongri Piao, Zhengkun Rong, Shuang Xu, Miao Zhang, and Huchuan Lu. Dut-lfsaliency: Versatile dataset and light field-to-rgb saliency detection. *arXiv preprint arXiv:2012.15124*, 2020.

[41] Yongri Piao, Zhengkun Rong, Miao Zhang, Weisong Ren, and Huchuan Lu. A2dele: Adaptive and attentive depth distiller for efficient rgb-d salient object detection. In *CVPR*, pages 9060–9069, 2020.

[42] Karen Simonyan and Andrew Zisserman. Very deep convolutional networks for large-scale image recognition. *arXiv preprint arXiv:1409.1556*, 2014.

[43] Hangke Song, Zhi Liu, Huan Du, Guangling Sun, Olivier Le Meur, and Tongwei Ren. Depth-aware salient object detection and segmentation via multiscale discriminative saliency fusion and bootstrap learning. *IEEE TIP*, 26(9):4204–4216, 2017.

[44] Ningning Wang and Xiaojin Gong. Adaptive fusion for rgb-d salient object detection. *IEEE Access*, 7:55277–55284, 2019.

[45] Xiaolong Wang and Abhinav Gupta. Unsupervised learning of visual representations using videos. In *ICCV*, pages 2794–2802, 2015.

[46] Zhou Wang, Eero P Simoncelli, and Alan C Bovik. Multiscale structural similarity for image quality assessment. In *The Thirty-Seventh Asilomar Conference on Signals, Systems & Computers*, 2003, volume 2, pages 1398–1402, 2003.

[47] Jing Zhang, Deng-Ping Fan, Yuchao Dai, Saeed Anwar, Fatemeh Sadat Saleh, Tong Zhang, and Nick Barnes. Uc-net: Uncertainty inspired rgb-d saliency detection via conditional variational autoencoders. In *CVPR*, pages 8582–8591, 2020.

[48] Jia-Xing Zhao, Yang Cao, Deng-Ping Fan, Ming-Ming Cheng, Xuan-Yi Li, and Le Zhang. Contrast prior and fluid pyramid integration for rgbd salient object detection. In *CVPR*, 2019.

[49] Xiaoqi Zhao, Lihe Zhang, Youwei Pang, Huchuan Lu, and Lei Zhang. A single stream network for robust and real-time rgbd salient object detection. In *ECCV*, pages 646–662, 2020.